PERGAMON

International Journal of Multiphase Flow 27 (2001) 1227–1245

International Journal of Multiphase Flow

www.elsevier.com/locate/ijmulflow

Collision of a droplet with a hemispherical static droplet on a solid

Hitoshi Fujimoto [a,*], Tomoyuki Ogino [a,1], Hirohiko Takuda [a], Natsuo Hatta [b]

[a] *Department of Energy Science and Technology, Graduate School of Energy Science, Kyoto University, Yoshida-Honmachi, Sakyo-ku, Kyoto 606-8501, Japan*

[b] *Department of Civil Engineering, Nippon-Bunri University, Ichigi, Oita 870-0397, Japan*

Received 16 February 2000; received in revised form 10 December 2000

Abstract

The collision of a liquid droplet with a hemispherical droplet on a horizontal smooth solid surface is studied experimentally as well as numerically. The hemispherical droplet is in the static state on the surface at room temperature and its volume is the same as an incoming droplet. The incoming droplet impinges vertically on the top of the hemispherical droplet. Qualitative and quantitative observations of the collision behavior of the liquid droplets are performed by means of a flash photographic method. The effect of impact velocity of the incoming droplet is investigated. It is found that a circular thin liquid film like a crown is formed around the bottom of the incoming droplet after the collision. The magnitude of the circular thin film becomes large with increasing the impact velocity. The collision behavior of liquid droplets is also analyzed numerically. The Navier–Stokes equations for incompressible viscous fluid in the axisymmetric coordinate system are solved by a finite difference method. The effects of viscosity, surface tension, and gravity are taken into account. The numerical results agree reasonably well with the experimental data. The hydrodynamics of the liquid is investigated to understand the physics of phenomena.

1. Introduction

Spray jet impingement on solid surfaces is utilized in various industrial applications such as mist or spray cooling, spray painting, spray coating, and ink jet printing. The flow fields of sprays impinging on the solid are very complex in nature because a number of liquid droplets interact

* Corresponding author. Tel.: +81-75-753-5419; fax: +81-75-753-5428.
E-mail address: h-fujimoto@energy.kyoto-u.ac.jp (H. Fujimoto).

[1] Present Address: Kawasaki Heavy Industries Corp.

0301-9322/01/$ - see front matter
PII: S0301-9322(00)00075-6

with each other near the solid surface. Up to now, the collision dynamics of a single droplet as well as multiple droplets with the solid surfaces has been studied for understanding the fundamental physics of phenomena (Rein, 1993; Chandra and Avedisian, 1991).

The collision behavior of a single droplet with the solid surface is strongly dependent upon several factors such as the Weber number associated with impact energy of droplet, the Reynolds number, the surface roughness of the solid, and the temperature of the solid surface (Rein, 1993). When a liquid droplet impacts the smooth solid surface with relatively large impact energy, the droplet splashes on it. On the other hand, no droplet disintegration occurs for the case of small impact energy. If the temperature of the solid surface is below the boiling temperature of liquid, the splash boundary depends upon the Weber number and the Reynolds number (Stow and Hadfield, 1981; Mundo et al., 1995). If the surface temperature is very high, the splash boundary is roughly given by the Weber number alone (Wachters and Westerling, 1966; Hatta et al., 1997). However, the knowledge obtained by the single droplet tests is not directly applicable to the actual flow fields of the spray jet impingement because the interaction effects of droplets are not included.

The collision of multiple droplets with a solid has also been studied experimentally as well as numerically. Yarin and Weiss (1995) observed the impact of liquid drops one by one on a solid surface by means of a CCD camera. The splashing threshold was studied. Liu et al. (1993) demonstrated the calculated deformation process of two droplets in tandem impinging on a solid surface. However, the collision dynamics of multiple droplets with the solid remains unclear because there are many parameters affecting the collision behavior (Rein, 1993).

The present study deals numerically as well as experimentally with the collision of water droplets one by one with a solid surface at room temperature. The simple case where the two droplets impinge vertically one by one on the solid surface with a very long time interval is treated. These droplets are of the same size. After the first droplet impinges onto the solid and reaches the steady state, the second droplet impacts the first droplet on the solid (see Figs. 1 and 2). The

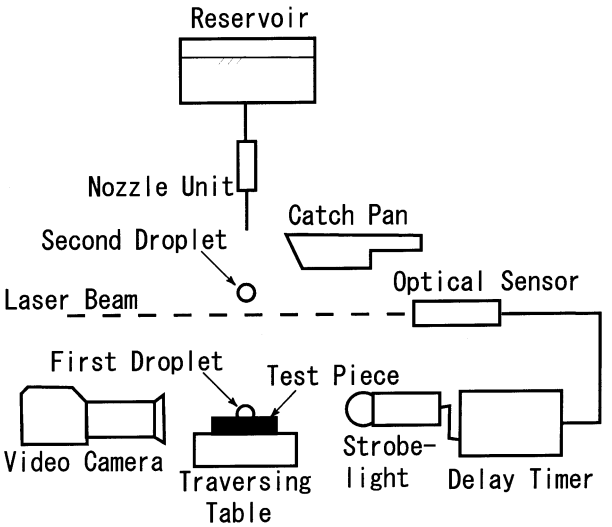

Fig. 1. Schematic of experimental apparatus to observe the collision behavior of droplets with a solid.

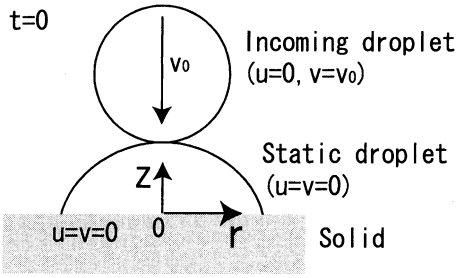

Fig. 2. Initial computational conditions and coordinate system.

interaction phenomena between the incoming droplet and the static droplet are investigated in detail.

First, the photographic observation is performed by means of a flash photographic method for several impact velocities. The effect of impact velocity on the collision behavior is examined. It is found that a circular thin liquid film like a crown is formed around the bottom of the incoming droplet after the collision. The magnitude of the circular thin film becomes large with increasing the impact velocity. Also, the off-centered collision of droplets is carried out.

Next, the deformation behavior of droplets is analyzed numerically. The Navier–Stokes equations for incompressible fluid in the axisymmetric coordinate system are solved by a finite difference method. The numerical simulations are performed only in the early time stages, in which a liquid crown is formed and spreads radially, because the appreciable three-dimensional nature of the flow is observed experimentally in the later time stages. The numerical results are compared with the experimental data for validating the present numerical model. The numerical results agree reasonably with the measured data. The detailed formation process of the liquid crown is studied from a numerical viewpoint. Also, the effect of surface tension as well as contact angle on the numerical results is investigated.

2. Experimental apparatus

Fig. 1 shows a schematic of the experimental apparatus to observe the collision behavior of liquid droplets with a solid. It consists of a nozzle unit to make uniform sized droplets, a test piece, optical devices (a video camera and a strobe light), an optical sensor and a delay timer to trigger the strobe light.

Distilled water at approximately 20°C is introduced into the top of the needle unit. A droplet is formed at the flat tipped nozzle and detaches under its own weight. A droplet with 2.4 mm diameter falls vertically and impinges onto a dry smooth solid surface made of optical glass (BK-7) at room temperature. The surface flatness, which is given by the difference between the peak and valley values of the surface height, is 600 nm (specified by the manufacturer). The test piece is fixed on a one-axis traversing table with ± 0.01 mm resolution. The droplet deforms like a thin circular disk on the surface, recoils, and finally becomes a hemispherical shape. After the droplet reaches the stationary state on the solid surface, the next droplet is formed at the needle and detaches. For convenience, the stationary droplet on the solid is called the first droplet, and the incoming

droplet is called the second droplet. The falling droplet (second droplet) passes though a laser beam to trigger the strobe light. Then, the second droplet impinges vertically onto the top of the static hemispherical droplet (first droplet) on the solid. The strobe light is operated with a preset delay time and the image of droplets is recorded. After the experiment, the wet surface is wiped carefully with dry clean tissues for the next experiment, so that the first droplets always impinge on the dry solid surface. Since droplets are formed periodically at the nozzle, the drop pan traps the incoming drops during wiping of the surface. After the solid surface is cleaned, the drop pan is removed for starting the next experiment. This procedure is repeated with different timings of flash under the same experimental condition.

A series of different droplets during the collision are recorded using a video camera (Canon XL1) with a macro lens. A strobe light (Sugawara MP-230A) is used as a light source for the video camera. The duration of flash is 2 μs (specified by the manufacturer). The video camera and the strobe light are set horizontally at the same level to the solid surface in order to take side-view photographs of droplets by a backlight method. The video camera is adjusted to effectively record the image only by the light of the flash. Also, the delay timer (Sugawara RE-306) controls the timing of flash with a resolution of 1 μs. The measurements of droplet dimensions are made directly from video images.

The impact velocity of droplets, which is controlled by the nozzle-to-surface distance, ranges between 0.8 and 3.1 m/s in the present study.

3. Conservation equations and numerical procedure

Fig. 2 shows a schematic of computational conditions and the coordinate system for analyzing the collision process of liquid droplets with a solid. The flow is regarded to obey the Navier–Stokes equations for incompressible viscous flow in the axisymmetrical coordinate system. The origin of the coordinate axes is set at the plate surface. In the present analysis, the effects of surface tension, viscosity, and gravity are taken into account. Isothermal conditions are assumed. The conservation equations of mass and momentum are as follows.

Continuity equation:

$$\frac{1}{r}\frac{\partial(ru)}{\partial r}+\frac{\partial v}{\partial z}=0. \tag{1}$$

Momentum equations in the radial and axial directions:

$$\rho\left(\frac{\partial u}{\partial t}+\frac{1}{r}\frac{\partial(ru^2)}{\partial r}+\frac{\partial(uv)}{\partial z}\right)=-\frac{\partial p}{\partial r}+\left(\frac{1}{r}\frac{\partial(r\tau_{rr})}{\partial r}+\frac{\partial\tau_{rz}}{\partial z}-\frac{\tau_\theta}{r}\right), \tag{2}$$

$$\rho\left(\frac{\partial v}{\partial t}+\frac{\partial uv}{\partial r}+\frac{\partial v^2}{\partial z}+\frac{uv}{r}\right)=-\frac{\partial p}{\partial z}+\rho F_z+\left(\frac{1}{r}\frac{\partial(r\tau_{rz})}{\partial r}+\frac{\partial\tau_{rz}}{\partial z}\right), \tag{3}$$

in which

$$\tau_{rr} = 2\eta\frac{\partial u}{\partial r}, \quad \tau_{rz} = \eta\left(\frac{\partial v}{\partial r} + \frac{\partial u}{\partial z}\right), \quad \tau_{zz} = 2\eta\frac{\partial v}{\partial z}, \quad \tau_{\theta} = 2\eta\frac{u}{r}, \tag{4}$$

where t, (r, z), (u, v), p, and ρ are the time, the coordinates in the radial and axial directions, the velocity components, the pressure, and the density, respectively. Also, F_z and η denote the gravitational acceleration and the viscosity, respectively.

The boundary conditions are explained next. The symmetric condition is imposed at the center axis. The zero velocity condition ($u = v = 0$) is adopted at the wall boundary. The Laplace equation is imposed at the free fluid surface,

$$p_s - p_a = \sigma\left(\frac{1}{R_1} + \frac{1}{R_2}\right), \tag{5}$$

in which p_s and p_a are the surface pressure and the atmospheric one, respectively. R_1 and R_2 are the principal radii of curvature at a point on the free liquid surface, respectively, and σ is the surface tension. Also, the condition that the tangential stress tensor is zero at the free liquid surface is used. The boundary condition as well as the numerical treatment at the contact line, which is defined by the free liquid surface on the solid, is described in the later part.

The numerical procedure is the same as that used in our previous study (Fujimoto et al., 1999). The flow fields are calculated using a finite difference method. The calculations are started when the incoming droplet (the second droplet) impinges on the top of the static hemispherical droplet (the first droplet) on the solid (see Fig. 2). It is assumed that the incoming droplet (the second droplet) is spherical in shape with no internal flow. The initial shape of the static hemispherical droplet is given by the experiments. As a matter of fact, the static hemispherical droplets are not always symmetric in the experiments, and depend upon the impact conditions (Fujimoto et al., 2000). Also, the shape is not always the same even under the same impact condition. Therefore, we have measured the shape of droplets in the stationary state five times for each experimental condition, and have determined the averaged droplet shape for the computational simulations.

The non-uniform grid system is employed to compute the flow in the liquid. The mesh size Δz in the axial direction is fine near the solid surface to capture the velocity boundary layer ($\Delta z/D_p = 5 \times 10^{-4}$ at the cell adjacent to the solid surface). In the other regions, the axial mesh size $\Delta z/D_p$ is 1/300. Also, the radial mesh size $\Delta r/D_p$ is set to 1/400 in the entire region. There are 800 grid lines in the radial direction and 450 grid lines in the axial direction. The grid convergence has been confirmed using a finer mesh with twice as many grid points for some cases in the early collision process. The time increment Δt is determined by the Courant–Friedrich–Levy (CFL) condition as

$$\Delta t = \min\left(\frac{f\,\Delta r}{(u + 2\eta/(\rho\Delta r))}, \frac{f\,\Delta z}{(v + 2\eta/(\rho\Delta z))}\right), \tag{6}$$

in which the CFL number f is set to 0.1 in this study. The effect of the time step on the numerical results has been checked by using $f = 0.05$ and 0.1 for some cases. It has been confirmed that the calculated flow fields using $f = 0.1$ coincide with the results using $f = 0.05$.

The time evolution of the free liquid surface is tracked by the Lagrangian movement of numerous consecutive segments (Hatta et al., 1995; Fujimoto and Hatta, 1996). The free surface positions at two consecutive time steps are formulated by

$$r_s^{n+1} = r_s^n + \Delta t u_s^n, \quad z_s^{n+1} = z_s^n + \Delta t v_s^n, \tag{7}$$

in which the subscript s represents the value at the free liquid surface. Eq. (7) is applied to every end-point of free surface segments except at the solid surface (contact line). Since the no-slip condition ($u = 0$) is imposed at the solid/liquid boundary, a special treatment is necessary at the contact line.

It is well known that the contact angle between the solid and the free liquid surface depends strongly upon the speed and the direction of the contact line movement. If the contact line advances along the surface, the contact angle increases, and in the case of receding movement, the contact angle decreases. A range of contact angles exists even at zero contact-line speed (hysterisis). In the present study, the computations are performed only in the early deformation stages when the contact line is first static and then increases to a constant advancing value. The advancing contact angle is set to 110° as observed experimentally. The computations are terminated before any significant decrease of contact line speed is observed.

The present numerical model treats the contact-angle hysteresis in the following manner: a tentative radial position of the free surface at the contact line is determined by a linear extrapolation from the two points of free liquid surface closest to the solid surface. If the calculated contact angle is smaller than the advancing one, the tentative contact line is regarded as the real contact line. Otherwise, the radial position of the contact line is adjusted to satisfy the advancing contact angle.

The predicted contact-line position obtained by this procedure remains almost constant if the liquid in the vicinity of the contact line is also stationary and the contact angle is smaller than the advancing one. If the fluid near the contact line begins to move, the predicted contact angle increases, and immediately reaches the advancing one. Also, the predicted contact angle is equal to the advancing one, when the contact line first advances following the liquid motion. This fact suggests that this numerical treatment can predict reasonably well the contact-angle transition from a small stationary contact angle to the advancing one.

4. Results and discussion

4.1. Experimental results

The photographic observations are performed to understand the collision dynamics of two droplets one by one onto the solid surface. The preimpact diameter of droplets is $D_p = 2.4$ mm. The impact velocity v_0 ranges from 0.8 to 3.1 m/s in order to investigate the effect of impact inertia on the collision dynamics. The solid surface area, on which the droplets impinge, is 21 mm × 15 mm. Fig. 3 shows sequences of photographs showing the deformation process of liquid droplets for $v_0 = 0.8$ m/s (a), 2.1 m/s (b), and 3.1 m/s (c), respectively. The time $t = 0$ s represents the moment at which the second droplet (incoming droplet) impacts on the top of the first droplet (static hemispherical droplet) on the solid.

For the case of $v_0 = 0.8$ m/s, it is seen that the liquid around the bottom of the second droplet swells up after the collision ($t = 0.7$ and 1.3 ms). The circular swelling part moves radially outward with time ($t = 0.7$ to 5.7 ms). Also, the liquid height near the center axis decreases monotonically.

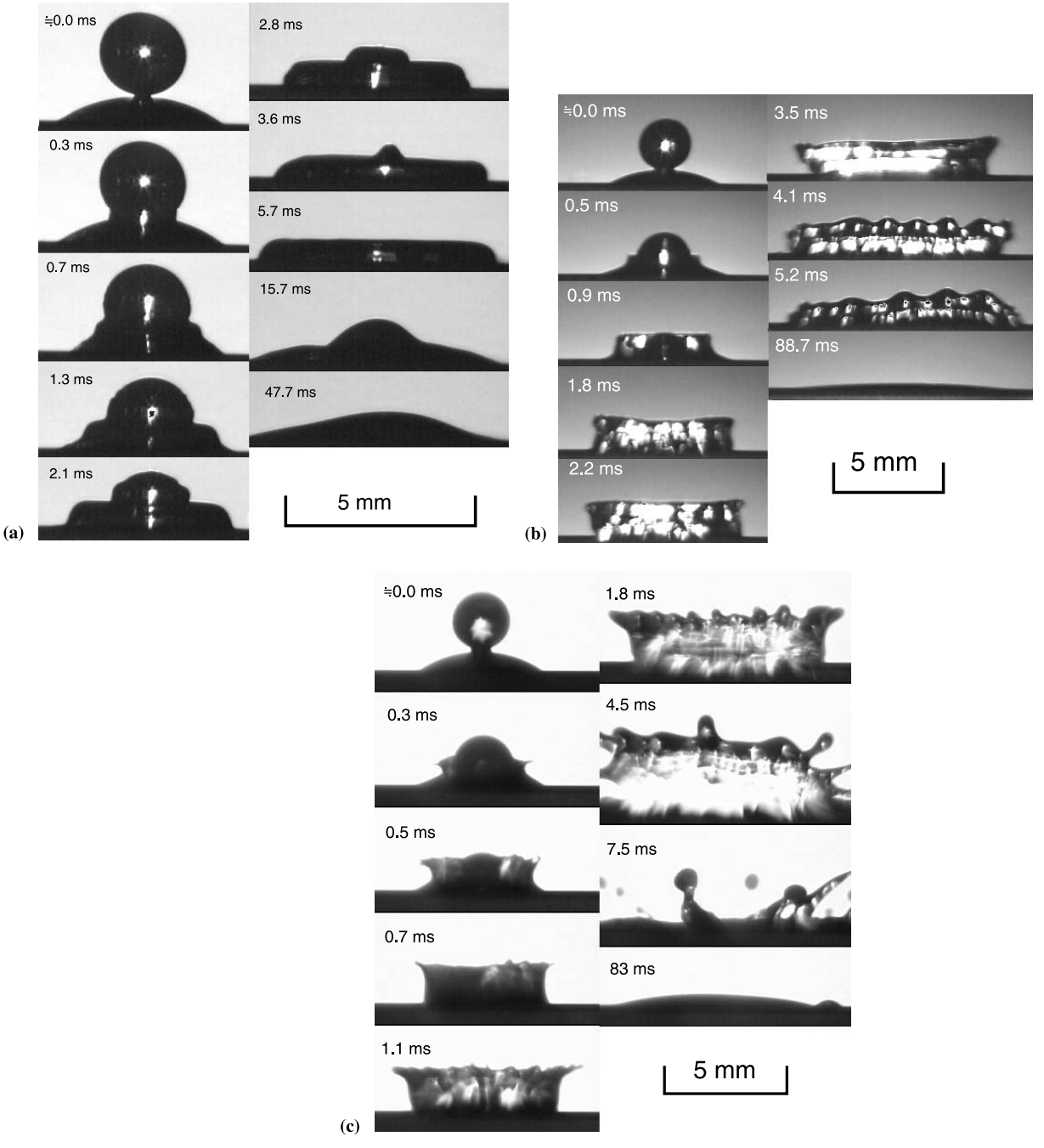

Fig. 3. Sequences of photographs showing the collision behavior of two droplets for the impact velocity $v_0 = 0.8$ m/s (a), 2.1 m/s (b), and 3.1 m/s (c), respectively. The preimpact diameter D_p is 2.4 mm.

Thus, the liquid is deformed like a thin circular disk on the solid. Also, the contact line defined by the free liquid surface at the solid surface stays in the same position until $t = 1.3$ or 2.1 ms, and then moves outward. This mechanism will be explained using the numerical results in the later subsection. The motion of the liquid decreases with time because of viscosity.

For the case of $v_0 = 2.1$ m/s, the thin circular liquid film appears around the body of the second droplet ($t = 0.5$ and 0.9 ms). The formation mechanism of the circular liquid film is discussed numerically in a later subsection. Since the liquid height near the center axis decreases with time due to inertia of the second droplet, the liquid is deformed like a crown on the solid ($t = 1.8$ to 2.2 ms). The liquid crown spreads radially with time. At $t = 3.5$ ms, the diameter of the liquid crown in the upper part becomes larger than that at the solid surface, because the spreading rate of the circular liquid film near the solid is smaller than that in the upper part due to wall friction. After that, the upper part of the circular liquid film is deformed like strings of beads ($t = 4.1$ ms) and then falls down radially outward ($t = 5.5$ ms). At $t = 88.7$ ms, the liquid thickness becomes very thin. The reason is due to the small surface area of the solid. In this case, the liquid diameter becomes larger than the short side length of the rectangular solid surface ($= 15$ mm) during the deformation. Since some part of contact line stays along both longer edges of the solid, the liquid becomes very thin in the later time stages.

The deformation process of liquid for $v_0 = 3.1$ m/s shows similar trends for $v_0 = 2.1$ m/s. The magnitude of the deformation scale is large compared with the previous one. It is seen that the circular liquid film is broken during the radially spreading process. Secondary droplets appear due to breaking of the crown ($t = 7.5$ ms). Anyway, it is confirmed from these results that the impact velocity strongly affects the collision dynamics of droplets.

Next the case where a single droplet impinges on a dry solid surface is examined to compare the deformation process of liquid for the case of two droplets. The impact condition is identical to the case of Fig. 3(b). Fig. 4 shows a sequence of photographs showing the deformation process of a single droplet on a dry solid. Time $t = 0$ s means the moment of impact. It is apparently seen that no liquid crown is formed in this case. The collision behavior is very different from the case of two droplets as shown in Fig. 3(b). The droplet height decreases monotonically with time in the present time stages, while the diameter of the droplet on the solid increases. Thus, it is confirmed that the formation of the liquid crown is the characteristic flow structure for the case of two droplets. The static droplet on the solid surface plays an important role in the formation of the liquid crown.

Cossali et al. (1997) studied the impact of a single drop onto a thin liquid film experimentally. They showed that a liquid crown is formed after the collision of the droplet with the liquid surface. Very recently, Weiss and Yarin (1999) studied the single drop impact onto liquid films numerically. The formation process of a liquid crown was simulated, although the viscosity effect was neglected. Therefore, the physics of phenomena for the present situation is similar not to the case of impact of a single droplet on a dry solid, but to the case for liquid surface. The detailed collision dynamics is discussed using numerical results in the later subsection.

In order to understand the effect of the impact velocity on the deformation process of liquid droplets quantitatively, the time evolution of the liquid height from the solid surface is measured for several impact velocities as shown in Fig. 5. The definition of the liquid height is shown in Fig. 6. It is also noted that the time t and liquid height H are normalized by D_p/v_0 and D_p, respectively. The liquid height decreases with time for every case after the collision. The decreasing rate of the

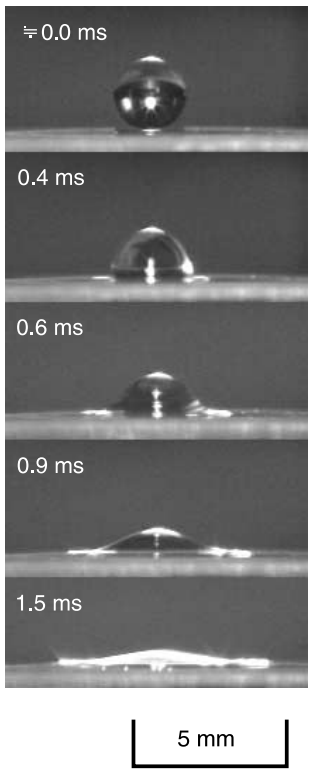

Fig. 4. A sequence of photographs showing the collision behavior of a single droplet with a dry solid. The impact condition is the same as the case of Fig. 3(b).

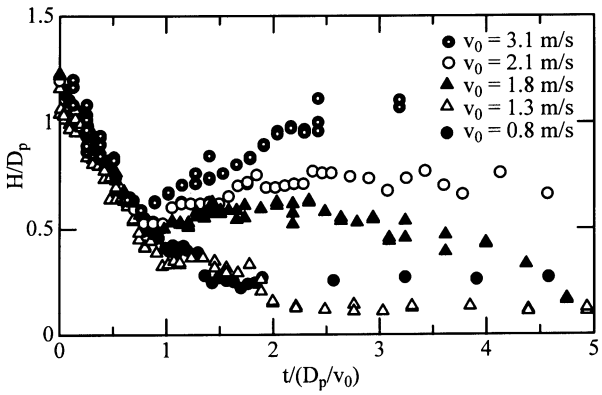

Fig. 5. Time evolutions of liquid height H/D_p from the solid surface for several impact velocities.

liquid height is equal to the impact velocity. For the cases of $v_0 = 1.8$, 2.1, and 3.1 m/s, the droplet height decreases, reaches a minimum value, and then increases. Before the droplet height reaches a minimum value, the droplet height at the center axis is higher than that of the circular film formed

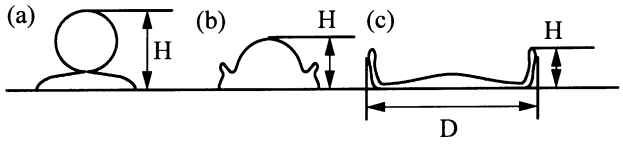

Fig. 6. Definition of liquid diameter D and liquid height H.

around the bottom of the second droplet (see Fig. 6(b)). At the moment of the minimum droplet height, the liquid height at the center axis is equal to that of the circular liquid film. After that, the circular liquid film becomes higher than the center part (see Fig. 6(c)). The time to reach the minimum droplet height becomes shorter for larger impact velocities. Also, the liquid height becomes higher for larger impact velocities. Subsequently, the droplet height reaches a maximum value, and then begins to decrease due to the gravitational effect. On the other hand, for the cases of $v_0 = 0.8$ and 1.3 m/s, the droplet height decreases monotonically with time, because the circular swelling part does not develop so high, as shown in Fig. 3(a).

Next, the off-centered collision of droplets is examined. Fig. 7 shows a sequence of photographs showing the off-centered collision process for $v_0 = 2.1$ m/s. These photographs are obtained by the following manner: After the first droplet impacts the solid and reaches the stationary state, the test surface fixed on the one-dimensional traversing table is moved to the left side by 1 mm very slowly so that the shape of the hemispherical liquid is not changed. Then, the second droplet impinges onto the first droplet. For convenience, the left side of the impact point of the second droplet in the photograph is called "thick film side", and the opposite is called "thin film side". In addition, the solid surface area, on which droplets impinge, is 21 mm $\times$ 21 mm. As expected, it is found that the liquid crown formed is asymmetric. The liquid film formed on the thick film side is higher than that on the thin film side ($t = 0.9$ to 2.2 ms). The contact line defined by the free liquid surface on the solid stays almost stationary on the thick film side till $t = 1.8$ ms. The deformation behavior of the liquid crown on the thin film side shows the similar trends as the case of two droplets (see Fig. 3(b)). On the other hand, the contact line on the thin film side moves radially outward with time. The liquid spreads along the dry solid surface. At $t = 3.1$ ms, the advancing part of liquid on the thin film side becomes roundish due to the surface tension effect. The spreading process of liquid on the thin film side is similar to the case of the impact of droplet on a dry solid as shown in Fig. 4. In addition, at $t = 97.6$ ms, the shape of the merged liquid is similar to the shape of the first droplet. Since the solid surface size is large enough, the spreading liquid does not reach any edge of the solid. The contact line reduces normally after the spreading rate of the liquid becomes zero. This is the reason why the shape of liquid in the later time stages is different from that for the case of Fig. 3(b).

4.2. Numerical results

First, the case where a single droplet impacts a dry solid is examined and predictions are compared with the experimental data in order to validate the present numerical model. The impact condition is the same as the case of Fig. 4. Fig. 8 shows the time evolution of the droplet shape and the velocity distribution calculated by the present numerical model. It is apparent that the predicted droplet shape during the collision agrees qualitatively well with the experimental

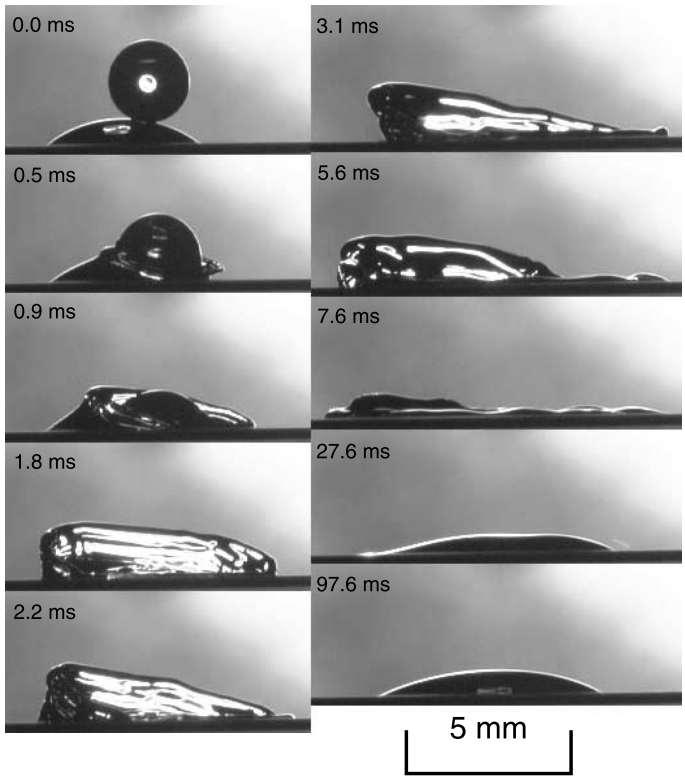

Fig. 7. A sequence of photographs showing the off-centered collision behavior of droplets for $v_0 = 2.1$ m/s. The impact condition is the same as the case of Fig. 3(b). Note that offset distance between the impact points of the first and second droplets is 1 mm.

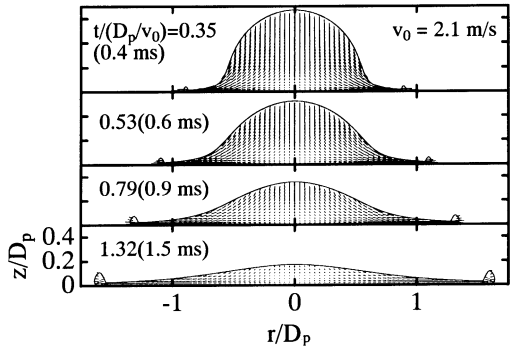

Fig. 8. Calculated deformation process of a liquid droplet impinging on a dry solid for $v_0 = 2.1$ m/s.

data. After the collision, the thin liquid film is formed around the bottom of the droplet. It spreads radially along the surface with time. Since the collision of a single droplet with a solid has already been studied numerically by some researchers (Fukai et al., 1995; Hatta et al., 1995; Pasandideh-Fard et al., 1996), the detailed deformation mechanism of the droplet is not discussed here.

Fig. 9 represents the comparison of predicted droplet dimensions with the experimental data. The definition of droplet dimensions is shown in Fig. 10. It is found that the time evolution of predicted D/D_p and H/D_p is in good agreement with the measured data in the present time scale.

Next, the case of two droplets is examined. Computer simulation is performed under the conditions of Fig. 3(b). Fig. 11 shows the time evolution of the shape of droplets, velocity distribution, and pressure contour inside the liquid, respectively, for $v_0 = 2.1$ m/s. The pressure contours are drawn at dimensionless pressures $(p - p_a)/\rho v_0^2 = 0.05i$ $(i = 1, 2, 3, \ldots)$. After the collision, the high pressure region appears near the stagnation point $(r/D_p, z/D_p) = (0, 0)$. Liquid around the bottom of the second droplet swells up, and it grows upward as well as radially outward with time. The liquid height near the center axis decreases monotonically. At $t/(D_p/v_0) = 0.79$, the circular liquid film becomes higher than the center part. After $t/(D_p/v_0) = 1.58$, the predicted liquid shape looks like a crown. The top part of the liquid crown becomes roundish because of the surface tension effect. Also, the pressure gradient inside the liquid is very small compared with that in earlier time stages.

The predicted deformation process of the liquid is similar to the experimental results as shown in Fig. 3(b) in the time range between 0.5 and 2.2 ms. The numerical results agree qualitatively well with the experimental data.

In order to validate the present numerical model quantitatively, the predicted liquid diameter as well as the liquid height is compared with the measured data. The predicted diameter of the circular liquid film defined in Fig. 5 is 2.89 at $t/(D_p/v_0) = 1.58$ and 3.04 at $t/(D_p/v_0) = 1.93$, while the experimental results are 2.64 at $t/(D_p/v_0) = 1.58$ and 2.94 at 1.93, respectively. Although the calculated diameter of the circular liquid film is a little larger than the measured data, the two results agree reasonably well with each other.

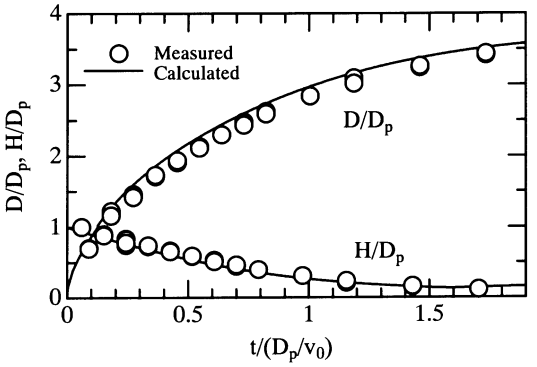

Fig. 9. Comparison of predicted droplet height and diameter on the solid surface with the experimental data.

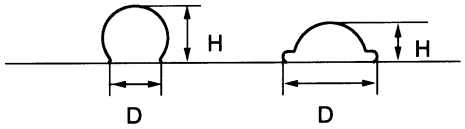

Fig. 10. Definition of liquid diameter D and liquid height H for the case of impact of a single droplet on a dry solid.

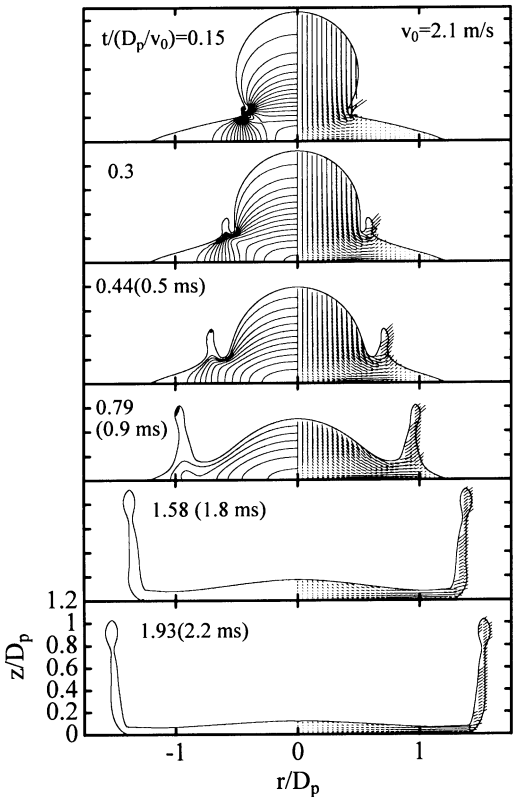

Fig. 11. Time evolution of predicted velocity and pressure profiles inside the liquid for $v_0 = 2.1$ m/s.

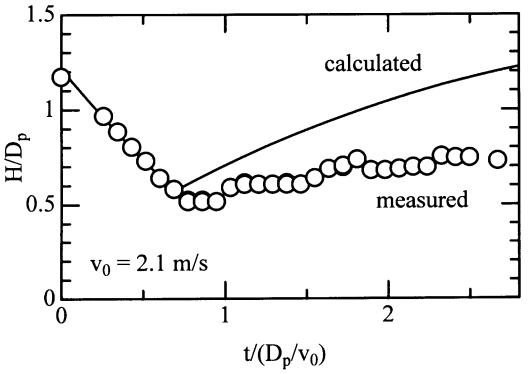

Fig. 12. Comparison of predicted droplet height H/D_p with the experimental data for $v_0 = 2.1$ m/s.

Fig. 12 shows the comparison of the predicted height of the liquid with the measurement data. It is found that the calculated results are in good agreement with the measured data just after the collision, but an appreciable discrepancy appears in later stages. The present numerical model overestimates the liquid height.

The reason why the discrepancy between the predicted and measured liquid heights appears for the case of two droplets is discussed. There are some possible reasons. The first reason is the three-dimensional nature of the flow in experiments. It is very difficult to insure perfect axisymmetric conditions experimentally. The initial shape of the static hemispherical droplet (the first droplet) is not always axisymmetric. Also, the three-dimensional nature of the flow is clearly seen in Fig. 3. The shapes of droplets are asymmetric, in particular, at later time stages. On the other hand, the present analysis has been performed using the two-dimensional flow model. No azimuthal flow is assumed. The momentum of the incoming droplet (the second droplet) gives rise to only the radial and axial flows in the numerical simulation. It is, therefore, expected that the predicted radial and axial velocity components become larger than the experimental ones.

The second reason is that the air flow surrounding the liquid is not taken into account. When the second droplet approaches the first one, the air between the first and second droplets is squeezed and the high-pressure air gap is built up. Some researchers reported that the entrapment

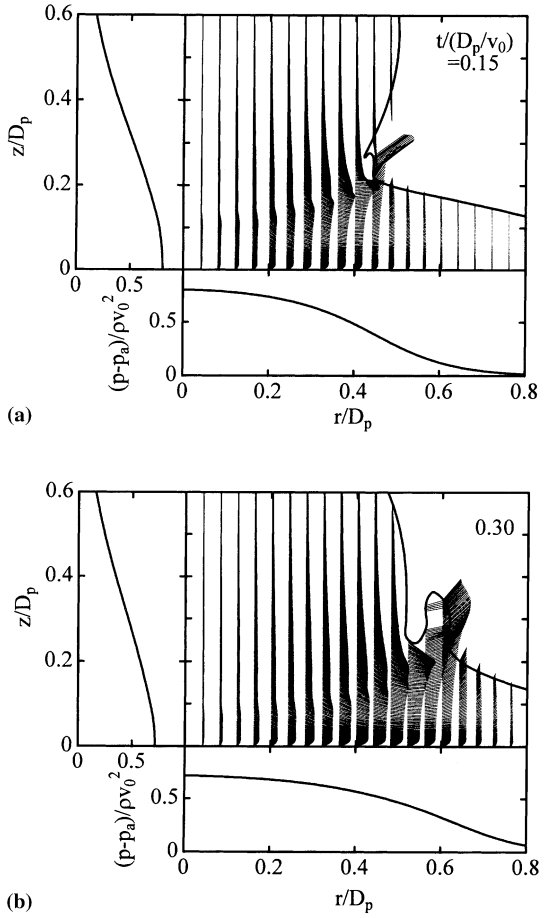

Fig. 13. Velocity profile near the stagnation point, and pressure distributions along the center axis and the solid surface at (a) $t/(D_p/v_0) = 0.15$ and (b) 0.3 for $v_0 = 2.1$ m/s.

of air occurs at the moment of the drop/drop impact or the drop/solid surface impact (Chandra and Avedisian, 1991; Rein, 1993; Fujimoto et al., 2000). Although we cannot observe the entrapment of air in the present experimental apparatus, some impact inertia may be lost due to the existence of the air gap.

Since the predictions are regarded to agree reasonably well with the experimental data, at least, in early time stages, the collision behavior of two droplets one by one with the solid is discussed in detail. The emphasis is placed upon the formation process of the liquid crown. Figs. 13(a) and (b) show the detailed velocity profile near the stagnation point, pressure distribution along the center axis and the solid surface at $t/(D_p/v_0) = 0.15$ and 0.3, respectively, for the case of $v_0 = 2.1$ m/s. It is found that the radial flow arises near the solid surface in the region of $r/D_p < 0.6$ at $t/(D_p/v_0) = 0.15$ due to the impact of the second droplet. The fluid is almost stagnant in the downstream region. The pressure is high at the stagnation point. It decreases with the radial and axial distances away from the stagnation point. A thin velocity boundary layer is formed from the stagnation point along the solid surface. The radial velocity component outside the boundary layer increases with r/D_p and then decreases. The radial velocity also increases axially with larger distance from the solid surface, and then decreases inside the second droplet. A strong oblique upward flow appears around the bottom of the second droplet near the free liquid surface.

The oblique flow is formed due to the following reason. The pressure at the free liquid surface is almost equal to the atmospheric one, while the pressure around the bottom of the second droplet

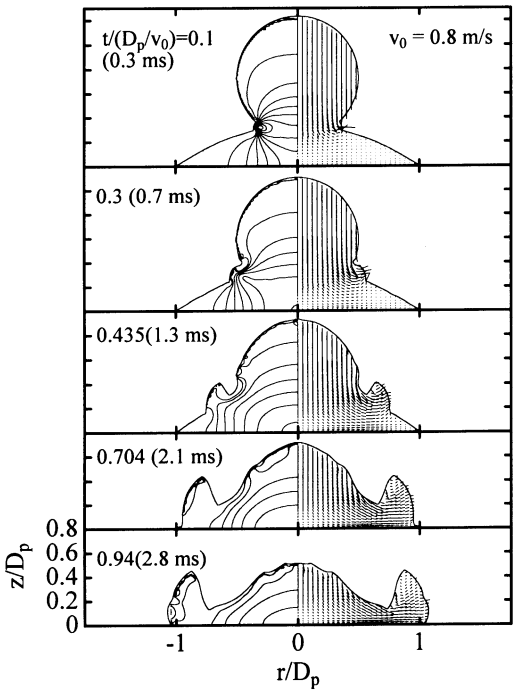

Fig. 14. Time evolution of predicted velocity and pressure profiles inside the liquid for $v_0 = 0.8$ m/s.

is high. The large pressure gradient normal to the free surface arises there (see also Fig. 11). The fluid is, therefore, accelerated obliquely upward.

At $t/(D_p/v_0) = 0.3$, the stagnation pressure becomes lower, and the radial velocity is larger than that at $t/(D_p/v_0) = 0.15$. Since the radial flow develops toward downstream along the solid surface, the stagnant fluid region becomes small. The upward flow near the free liquid surface arises in the region of $r/D_p = 0.6$ to 0.7 due to the stagnant fluid. It is seen in Fig. 11 that the axial pressure gradient is relatively large at the bottom of the circular swelling part at $r/D_p \approx 0.6$. Therefore, the pressure gradient gives rise to the upward motion of the liquid crown.

The stagnant fluid region downstream of the liquid crown appears until $t/(Dp/v_0) \sim 0.79$ (see Fig. 11). The axial pressure gradient near the bottom of the liquid crown is relatively large in this time range. Thus, the upward flow continuously arises there. After the stagnant fluid region vanishes, no driving force for upward motion of the liquid is exerted. But, the liquid crown continues to move upward because of its inertia. Thereby, the high circular liquid crown is formed for the case of $v_0 = 2.1$ m/s.

Next, the case of $v_0 = 0.8$ m/s is examined. Fig. 14 shows the time evolution of the velocity and pressure profiles inside the liquid. The calculated deformation process of the liquid agrees qualitatively well with the experimental data as shown in Fig. 3(a). It is found that the velocity profiles and pressure contours just after the collision are similar to those for the case of $v_0 = 2.1$ m/s. At $t/(D_p/v_0) = 0.1$ and 0.23, the pressure is high at the stagnation point. It decreases with radial and axial distances. Large pressure gradient appears at the free liquid surface around the bottom of the second droplet. However, the subsequent deformation process is apparently different from the case of $v_0 = 2.1$ m/s. The circular liquid crown formed is thick and not so high, because the effects

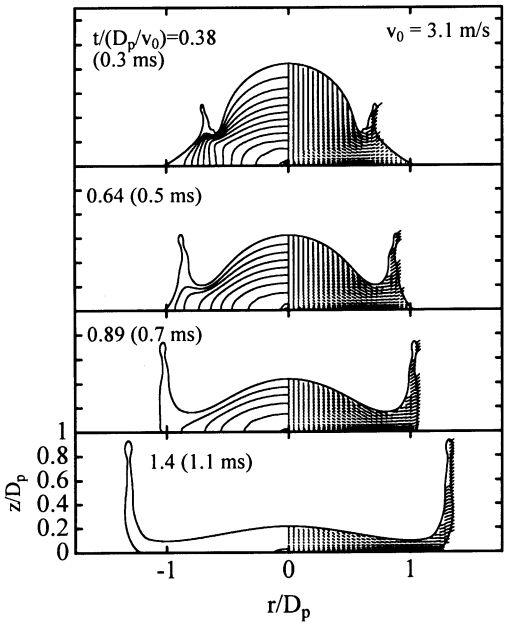

Fig. 15. Time evolution of predicted velocity and pressure profiles inside the liquid for $v_0 = 3.1$ m/s.

of viscosity and surface tension on the liquid motion become relatively large due to the small initial momentum of the second droplet. The contact line is static until $t/(D_p/v_0) \cong 0.704$ since the fluid in the vicinity of the contact line is at rest. The fluid near the contact line begins to move when the spreading circular crown reaches there. Consequently, the contact line advances following the liquid motion.

Fig. 15 shows the collision behavior of droplets for $v_0 = 3.1$ m/s. The predicted time evolution of liquid shape agrees qualitatively well with the experimental data as shown in Fig. 3(c). It is numerically found that the velocity profile and the pressure distribution inside the liquid are very similar to those for $v_0 = 2.1$ m/s. Since the initial momentum of the second droplet is larger than that for $v_0 = 2.1$ m/s, the magnitude of the deformation scale of liquid is, as expected, larger.

The sensitivity of the advancing contact angle to the numerical results is discussed next. The case of the single droplet impact is treated first. Fukai et al. (1995) shows that the advancing contact angle has some effect on the time evolution of the droplet diameter. The spreading diameter of the droplet becomes larger with smaller advancing contact angle. The effect of the advancing contact angle appears clearly with decreasing the spreading rate of the contact line.

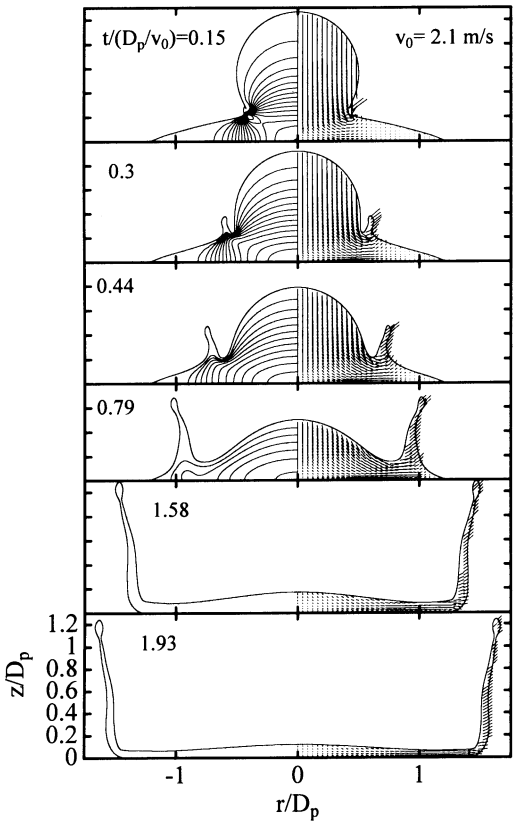

Fig. 16. Time evolution of predicted velocity and pressure profiles inside the liquid for $v_0 = 2.1$ m/s. Note that the surface tension is as half as that used in Fig. 11.

In order to investigate the contact-angle effect, the deformation behavior of a single droplet onto a solid is calculated for $v_0 = 2.1$ m/s and the contact angle = 60°. The numerical results are compared with the results for 110°. It is noted that the calculated contact angle becomes always equal to the advancing one for the case of a single droplet, because the contact line advances continuously. It is found that the predicted droplet diameter for the small contact angle ($= 60°$) becomes about 4% larger than that for 110° at $t/(D_p/v_0) = 1.5$. The difference between two droplet diameters is not so large, because the impact inertia is still dominant in this time stage. The results are consistent with Fukai et al. data.

A similar comparison is made in the case of two droplets for $v_0 = 2.1$ m/s. At $t/(D_p/v_0) = 1.93$, the difference between two predicted radial positions of the contact line for 60° and 110°, is about 1%. The reason why the difference is very small is discussed here. The contact line does not move until the fluid in the vicinity of the contact line begins to move at about $t/(D_p/v_0) = 1.2$. The contact angle is smaller than the advancing one up to that time. Therefore, the advancing contact angle never affects the liquid motion. After the contact line begins to move, the contact angle immediately becomes the advancing one. But, the inertia of the radially outward flow is dominant for a while. Thus, the advancing contact angle has little effect on the liquid motion in the early time stages. Anyway, it is confirmed that the advancing contact angle has a slight effect on the predicted liquid motion in very early time stages.

Finally, the effect of surface tension on the liquid motion is investigated numerically. The computation is carried out for $v_0 = 2.1$ m/s using a small surface tension, which is as half as that we have used. Fig. 16 shows the time evolution of the velocity and pressure profiles inside the liquid. It is found that both the velocity profile and the pressure distribution are very similar to those as shown in Fig. 11. But, the thickness, the height, and the diameter of the crown are thinner, taller, and larger than those in Fig. 11. The surface tension plays a role in reducing the development of the liquid crown.

5. Conclusion

The impact of two droplets one by one upon a solid, with a long time interval has been studied experimentally as well as numerically. It has been experimentally found that the circular liquid crown has been formed after the impact of the second droplet on the top of the static first droplet for relatively large impact velocities. The liquid crown becomes high for larger impact velocities. For the case of off-centered collisions, the flow is asymmetric. Next, the collision behavior of droplets with the solid has been investigated numerically. The predictions agree reasonably well with the experimental data. The formation process of the liquid crown is discussed in detail. It has been confirmed that the circular liquid crown is formed due to a large pressure gradient near the free surface. The stagnant first droplet on the solid plays an important role for the formation of the crown.

Acknowledgements

This study has been supported by Grant-in-Aid for Scientific Research (B)(2) (11450274) which is provided by the Ministry of Education, Science, Sports and Culture in Japan.

References

Chandra, S., Avedisian, C.T., 1991. On the collision of a droplet with a solid surface. Proc. R. Soc. London, Ser. A 432, 13–41.

Cossali, G.E., Coghe, A., Marengo, M., 1997. The impact of a single drop on a wetted solid surface. Exp. Fluids 22, 463–472.

Fukai, J., Shiiba, Y., Yamamoto, T., Miyatake, O., Poulikakos, D., Megaridis, C.M., Zhao, Z., 1995. Wetting effects on the spreading of a liquid droplet colliding with a flat surface: experimental and modeling. Phys. Fluids 7, 236–247.

Fujimoto, H., Hatta, N., 1996. Deformation and rebounding processes of a water droplet impinging on a flat surface above the Leidenfrost temperature. Trans. ASME J. Fluids Eng. 118, 142–149.

Fujimoto, H., Hatta, N., Viskanta, R., 1999. Numerical simulation of convective heat transfer to a radial free surface jet impinging on a hot solid. Heat Mass Transfer 35 (4), 266–272.

Fujimoto, H., Shiraishi, H., Hatta, N., 2000. Evolution of liquid/solid contact area of a drop impinging on a solid surface. Int. J. Heat Mass Transfer 43-4 (4), 1673–1677.

Hatta, N., Fujimoto, H., Takuda, H., 1995. Deformation process of a water droplet impinging on a solid surface. Trans. ASME J. Fluids Eng. 117, 394–401.

Hatta, N., Fujimoto, H., Kinoshita, K., Takuda, H., 1997. Experimental study of deformation mechanism of a water droplet impinging on hot metallic surfaces above the Leidenfrost temperature. Trans. ASME J. Fluids Eng. 119, 692–699.

Liu, H., Lavernia, E.J., Rangel, R.H., 1993. Numerical simulation of substrate impact and freezing of droplets in plasma spray processes. J. Phys. D: Appl. Phys. 26, 1900–1908.

Mundo, Chr., Sommerfeld, M., Tropea, C., 1995. Droplet-wall collisions: experimental studies of the deformation and breakup process. Int. J. Multiphase Flow 21, 151–173.

Pasandideh-Fard, M., Qiao, Y.M., Chandra, S., Mostaghimi, J., 1996. Capillary effects during droplet impact on a solid surface. Phys. Fluids 8, 650–659.

Rein, M., 1993. Phenomena of liquid drop impact on solid and liquid surfaces. Fluid Dyna. Res. 12, 61–93.

Stow, C.D., Hadfield, M.G., 1981. An experimental investigation of fluid flow resulting from the impact of a water drop with an unyielding dry surface. Proc. R. Soc. London, Ser. A 373, 419–441.

Wachters, L.H.J., Westerling, N.A.J., 1966. The heat transfer from a hot wall to impinging water drops in the spheroidal state. Chem. Eng. Sci. 21, 1047–1056.

Weiss, D.A., Yarin, A.L., 1999. Single drop impact onto liquid films: neck distortion, jetting, tiny bubble entrainment, and crown formation. J. Fluid Mech. 385, 229–254.

Yarin, A.L., Weiss, D.A., 1995. Impact of drops on solid surfaces: self-similar capillary waves, and splashing as a new type of kinematic discontinuity. J. Fluid Mech. 283, 141–173.